

See discussions, stats, and author profiles for this publication at: <https://www.researchgate.net/publication/320100545>

# Differential voltage analysis as a tool for analyzing inhomogeneous aging: A case study for LiFePO<sub>4</sub>|Graphite cylindrical cells

Article in Journal of Power Sources · September 2017

DOI: 10.1016/j.jpowsour.2017.09.059

CITATIONS

5

READS

296

## 4 authors:



[Meinert Lewerenz](#)

Technische Hochschule Ingolstadt

18 PUBLICATIONS 48 CITATIONS

[SEE PROFILE](#)



[Andrea Marongiu](#)

FEV Italia s.r.l.

18 PUBLICATIONS 186 CITATIONS

[SEE PROFILE](#)



[Alexander Warnecke](#)

HELLA Group

16 PUBLICATIONS 196 CITATIONS

[SEE PROFILE](#)



[Dirk Uwe Sauer](#)

RWTH Aachen University

597 PUBLICATIONS 6,023 CITATIONS

[SEE PROFILE](#)

Some of the authors of this publication are also working on these related projects:



Project Simulationsmodell zur Maximierung der Lebensdauer für Bleibatterien zum Ausgleich von fluktuierenden erneuerbaren Energien [View project](#)



Project Energy System Analysis at ISEA [View project](#)

Full Paper can be found for free until November 18, 2017 here

<https://authors.elsevier.com/a/1VoaB1M7w0FFKK>

Afterwards full paper is found here:

<http://www.sciencedirect.com/science/article/pii/S0378775317312788>

**Title: Differential voltage analysis as a tool for analyzing inhomogeneous aging: a case study for LiFePO<sub>4</sub>|Graphite cylindrical cells**

## Authors

Meinert Lewerenz<sup>a,b</sup>, Andrea Marongiu<sup>a,b</sup>, Alexander Warnecke<sup>a,b</sup> and Dirk Uwe Sauer<sup>a,b,c</sup>

## Affiliation

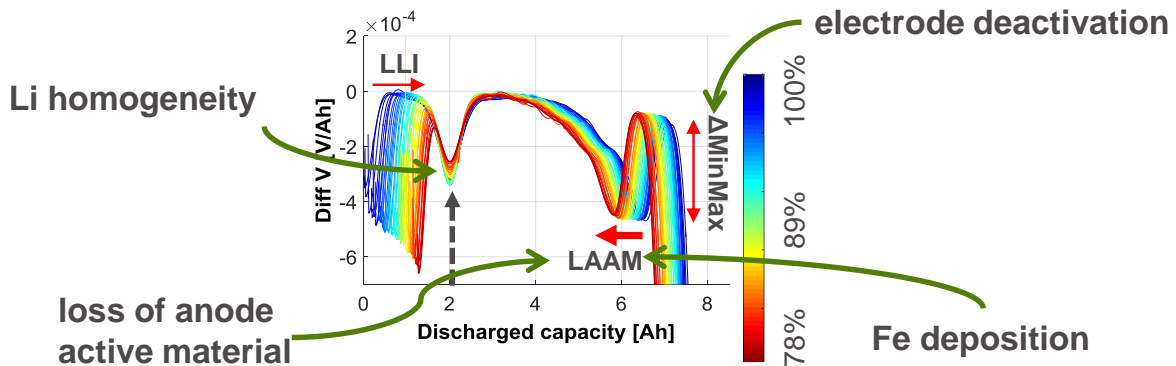
a) Electrochemical Energy Conversion and Storage Systems Group, Institute for Power Electronics and Electrical Drives (ISEA), RWTH Aachen University, Jägerstrasse 17/19, D-52066 Aachen, Germany

b) Juelich Aachen Research Alliance, JARA-Energy, Germany

c) Helmholtz Institute Münster (HI MS), IEK-12, Forschungszentrum Jülich, Corrensstrasse 46, 48149 Münster, Germany

## Key Words

Fe dissolution, deactivation of electrodes, deposition layer, loss of anode active material; lithium distribution



## Abstract

In this work the differential voltage analysis (DVA) is evaluated for  $\text{LiFePO}_4|\text{Graphite}$  cylindrical cells aged in calendaric and cyclic tests. The homogeneity of the active lithium distribution and the loss of anode active material (LAAM) are measured by the characteristic shape and peaks of the DVA. The results from this analysis exhibit an increasing homogeneity of the lithium-ion distribution during aging for all cells subjected to calendaric aging. At  $60\text{ }^\circ\text{C}$ , LAAM is found additionally and can be associated with the deposition of dissolved Fe from the cathode on the anode, where it finally leads to the clogging of pores. For cells aged under cyclic conditions, several phenomena are correlated to degradation, such as loss of active lithium and local LAAM for 100% DOD. Moreover, the deactivation of certain parts of anode and cathode due to a lithium-impermeable covering layer on top of the anode is observed for some cells. While the 100% DOD cycling is featured by a continuous LAAM, the LAAM due to deactivation by a covering layer of both electrodes starts suddenly. The homogeneity of the active lithium distribution within the cycled cells is successively reduced with deposited passivation layers and with LAAM that is lost locally at positions with lower external pressure on the electrode.

## Abbreviations

- |      |                               |
|------|-------------------------------|
| FCE: | full cycle equivalents        |
| DVA: | differential voltage analysis |

PMA:	post-mortem-analysis
EC:	ethylene carbonate
DMC:	dimethylene carbonate
EMC:	ethylene-methylene carbonate
DEC:	diethylene carbonate
LFP:	lithium iron phosphate
HLD:	homogeneity of lithium distribution
SEI:	solid electrolyte interphase
DOD:	depth of discharge
SOC:	state of charge
PEE:	passive electrode effect
CDA:	capacity difference analysis
LLI:	loss of lithium inventory (loss of active lithium)
LAAM:	loss of anode active material
MinHi:	minimum at high SOC
MinLo:	minimum at low SOC
MaxLo:	maximum at low SOC
$\Delta$ Minima:	$\text{MinLo}(x) - \text{MinHi}(x)$
$\Delta$ MinMax:	$\text{MaxLo}(y) - \text{MinLo}(y)$

## 1. Introduction

Nowadays it is of greater interest in industry and research to be able to characterize industrial lithium-ion batteries without having the effort and costs of cell disassembling. Therefore, a non-destructive method should describe the dominating aging mechanisms and the state of health with respect to extractable capacity and power capability. Furthermore an ex-situ method should give information especially about the lateral homogeneity of the cell with respect to loss of active material and lithium distribution.

Assuming a homogeneous electrode coating and a homogeneous pore size distribution of the separator, the homogeneity of the lithium distribution is strongly depending on the boundary conditions in a certain cell design, such as pressure on electrode stack [1], winding radius and distribution of anode overhang [2,3]. Especially for cylindrical cells the conditions vary from the core to the shell of the jelly roll and from the center to the edges of the electrodes. Furthermore the double-sided electrodes are compressed by curvature facing the core and are uncompressed facing the shell. Some authors in literature investigated and described inhomogeneously aged electrodes in a post-mortem-analysis [4,1]. Osswald et al. [5] evaluated the local cell potentials in a cylindrical cell. However, to our knowledge, studies explaining the different aging mechanism in a cell constrained by its cylindrical design are missing.

Increasing or decreasing homogeneity in lithium distribution is hardly addressed in literature. The degree of homogeneity with respect to active lithium distribution during aging can lead to different phenomena. A considerably low homogeneity might lead to less extractable capacity due to reaching the cut-off voltage earlier, or even lithium plating during charging. However, no publication discussing these considerations is known to the authors. Local lithium plating can in a late stage of degradation lead to the evolution of a dense covering layer [6]. The presence of a dense covering layer, reported in several publications [2,4,7,8], can result at the beginning in masking of the surface and by this to an inhomogeneous lithium distribution. This is supported by Cannarella et al. [9] for defects in the form of a

separator with closed pores. If the covering layer is passivated and finally becomes impermeable to lithium-ions within even a low current discharge, the covered anode and the opposed cathode are not chargeable or dischargeable anymore. This can be considered as if the electrode area is ‘deactivated’ in vertical direction [6,10].

Furthermore, especially in graphite-based anodes, a high depth of discharge (DOD) is strictly related to a high volume change (up to 10% [11]) depending on the porosity of the electrode. The volume change leads in most cells to the loss of active material (LAAM) [12]. If the LAAM appears only locally instead of uniformly, the homogeneity of lithium distribution will be reduced, too. A publication that discusses the LAAM by the constraints of a cylindrical cell is not known to the authors.

Exactly the same cylindrical LiFePO<sub>4</sub>|Graphite cells that are examined in this contribution have already been evaluated ex-situ by some authors of this work based on capacity loss, increase of internal resistance [2], capacity difference analysis (CDA) [10] and evaluation of floating currents [13]. The results of these evaluations are therefore placed in the context of the previously discussed techniques and the post-mortem-analyses that were applied to these cells. The aim of this work, however, is to further analyze the calendaric and cyclic aging of the 50 LiFePO<sub>4</sub>|Graphite cylindrical cells introduced earlier, by means of the widely used differential voltage analysis (DVA) technique. The key advantage of the DVA is that the loss lithium inventory (LLI), the LAAM [14,15] and the homogeneity of the charge distribution are quantitatively measurable. The DVA returns no direct information about the LiFePO<sub>4</sub> cathode due to its flat voltage characteristics.

The following sections of this work are organized as follows: The calendaric aging is presented in section 4.1, discussing the increasing homogeneity during aging and the influence of Fe dissolution and deposition on the anode for 60 °C tests. In section 4.2, the results for the cyclic aging are presented and evaluated according to the homogeneity of lithium distribution and LAAM. Finally, strong inhomogeneities in DVA are linked to the local deactivation of electrodes by covering layer evolution.

## 2. Experimental

### 2.1 Cells, aging and check-ups

A description of the tested cells and the experimental procedure has already been presented by the authors in [2], and the most important information are recapped in the following. 50 cylindrical high-power 8 Ah cells are tested. The cell comprises LiFePO<sub>4</sub> (LFP) on the cathode, graphite on the anode, and the composition (EC-DMC-DEC-EMC)-LiPF<sub>6</sub> as electrolyte. The tests are divided into calendaric (Table 1) and cyclic (Table 2) aging tests. The aging is interrupted at regular intervals for check-ups measuring the internal resistance, the capacity at 1C (capacity test) and a low current discharge at 0.25 C used for DVA. During check-up the temperature is set to 25 °C. The current capacity is defined at a C-rate of 1C. All SOC are approached Ah-based. Only the 100 % tests are floated at a voltage of 3.6 V, as the voltage curve at a lower SOC is rather flat to fix the SOC by a certain voltage in a practical setup.

**Table 1 Matrix of calendaric aging test and the number of cells for the corresponding test.**

SOC	25 °C	40 °C	60 °C
20%		3	
50%	3	3	3
80%		3	
100%	3	3	3

The capacity test is conducted as follows. After the cell is charged with 1C (8 A) up to 3.65 V, followed by constant-voltage charging down to  $I < 0.05C$  (maximum 2 h), the low current discharge at 0.25C is carried out until a cutoff voltage of 2 V is reached. After a pause of 1 h, the cell is recharged with 0.25C up to 3.65 V. The low current discharge curve is used for DVA. To achieve a good result after differentiation, the data is smoothed with a moving average to overcome quantization of the voltage measurement. The smoothed data is fitted

with a spline function and thereafter the derivative is calculated. Thus, a rather smooth result is achieved without influencing the shape and peak information. In some graphs the limits of a spline function are visible by superposition of a sine curve. This is due to the limitations of a function fitting with high slopes at the beginning and at the end of the curve, and nearly zero slope in-between. Therefore, the parameters for the fitting function are optimized to achieve an acceptable fit result over a wide SOC range.

All cycling tests have a mean SOC of 50%. After a complete charge process, the mean SOC of the corresponding cycle, defined using the current capacity, is approached Ah-based, due to the flat open circuit voltage (OCV) curve which characterizes LiFePO<sub>4</sub> cells. The only exception is the 1C 100% DOD test, which needs to be conducted voltage-based. The cells are cycled Ah-based around the mean SOC of the cycling, while the DOD is related to the nominal capacity, i.e. the DOD is not adapted to the current capacity. The temperature chamber was adjusted to ensure a cell temperature of 40 °C measured at the cell case.

**Table 2 Matrix of cyclic aging test and the number of cells for the corresponding test.**

C-rate	DOD		
	100%	50%	10%
1C	3	9	3
2C		3	
4C		3	
8C		5	

## 2.2 Post-Mortem Analysis

The post-mortem analyses are performed under argon atmosphere in a fully discharged or fully charged state. The cells are evaluated by their surface morphology and color using a Keyence VK-9710 laser microscope (confocal microscope).

The lithium distribution is measured with Varian ICP-OES (inductively coupled plasma-optical emission spectrometer), shortened to ICP. Therefore 15 spatially distributed discs of the double-coated electrodes, with a diameter of 20 mm, are taken. As preparation each sample is washed with DMC before it is dissolved in aqua regia.

For half-cell tests, one electrode side is removed and then 15 samples per electrode with a diameter of 16 mm are mounted in a coin cell vs. lithium metal. Whatman GF-C is used as separator. The check-up capacities are evaluated at C-rate of 0.1C for the anode in the range of 5 mV to 2.0 V and for the cathode in the range of 1.8 V to 3.8 V. The cells are cycled using a BaSyTec CTS system.

### 2.3 DVA evaluation strategy

The DVA is carried out for all constant current discharge curves of the full cell measured at each check-up. Special characteristic points are evaluated for each curve as illustrated in Figure 1: these are the minimum at high SOC (MinHi), the minimum at low SOC (MinLo) and the maximum at low SOC (MaxLo). Meaningful relative values turned out to be, on the one hand, the Ah-distance between the minima:

$$\Delta\text{Minima} = \text{MinLo}(x) - \text{MinHi}(x) \quad (1)$$

and, on the other hand, the difference between the minimum and maximum of the identified peaks at low SOC:

$$\Delta\text{MinMax} = \text{MaxLo}(y) - \text{MinLo}(y) \quad (2)$$

While  $\Delta\text{MinMax}$  can be analyzed over the entire test,  $\Delta\text{Minima}$  is only determinable as long as enough active lithium is available to reach the necessary degree of lithiation of the graphite to measure MinHi [16–18]. This is generally the case where the capacity goes down to approx. 75-80% remaining capacity when only loss of active lithium takes place (Figure 1c).

The shape of the DVA is basically originated from the anode curve as the LiFePO<sub>4</sub> cathode exhibits a flat voltage characteristic during most of the discharge process (Figure 1b). Therefore, the trend of  $\Delta\text{Minima}$  can be correlated directly to the capacity of the anode. This

correlation is reported in many publications [17–20]. In case of high inhomogeneities of lithium distribution, the curve shape might change significantly (as shown in section 4.2.3).

Besides the already named characteristic points, the curve shape will be qualified by the sharpness (or shape) of the MinHi peak and the detectability of the two shoulders recognizable at MinLo peak. A quantification of the homogeneity of lithium distribution (HLD) or aging is possible evaluating only the peak characteristics (position and shape) of MinHi in a rather homogenized state of the cell.

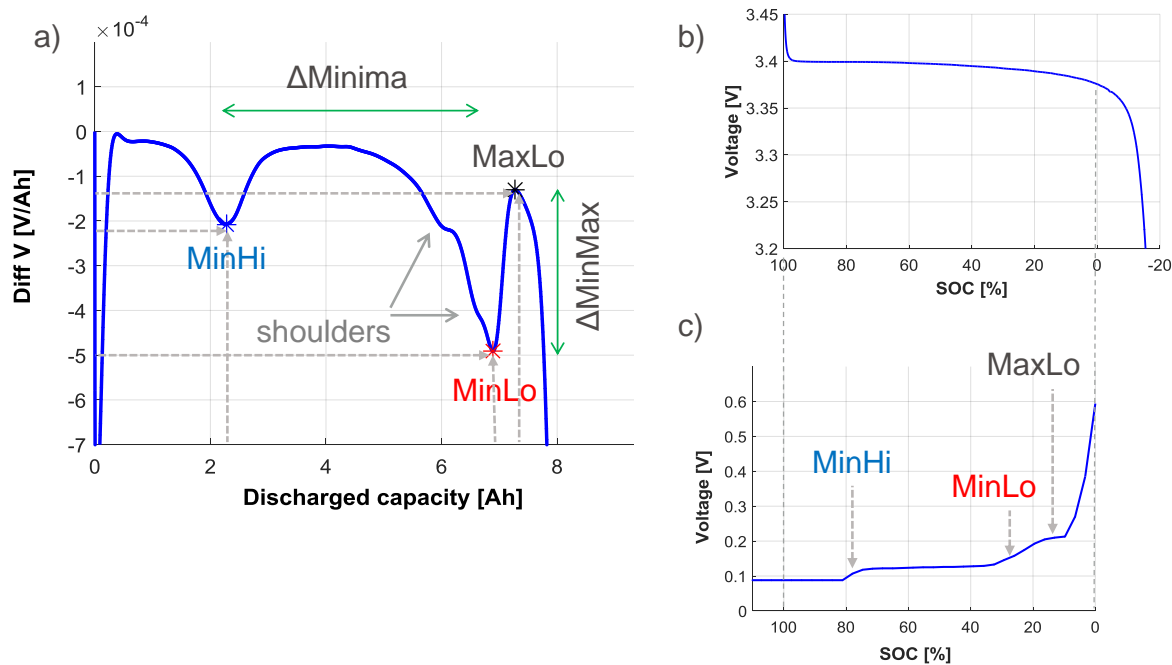


**Figure 1** a) Representation of a DVA curve including the characteristic measurands evaluated in this contribution; b) a slow discharge curve of the cathode and c) OCV-Voltage curve of an anode half-cell with allocation of the characteristic minima and maximum. The anode and the cathode are shifted to each other due to loss of SEI during formation [14]. The SOC is referred to the full cell.

### 3. Results

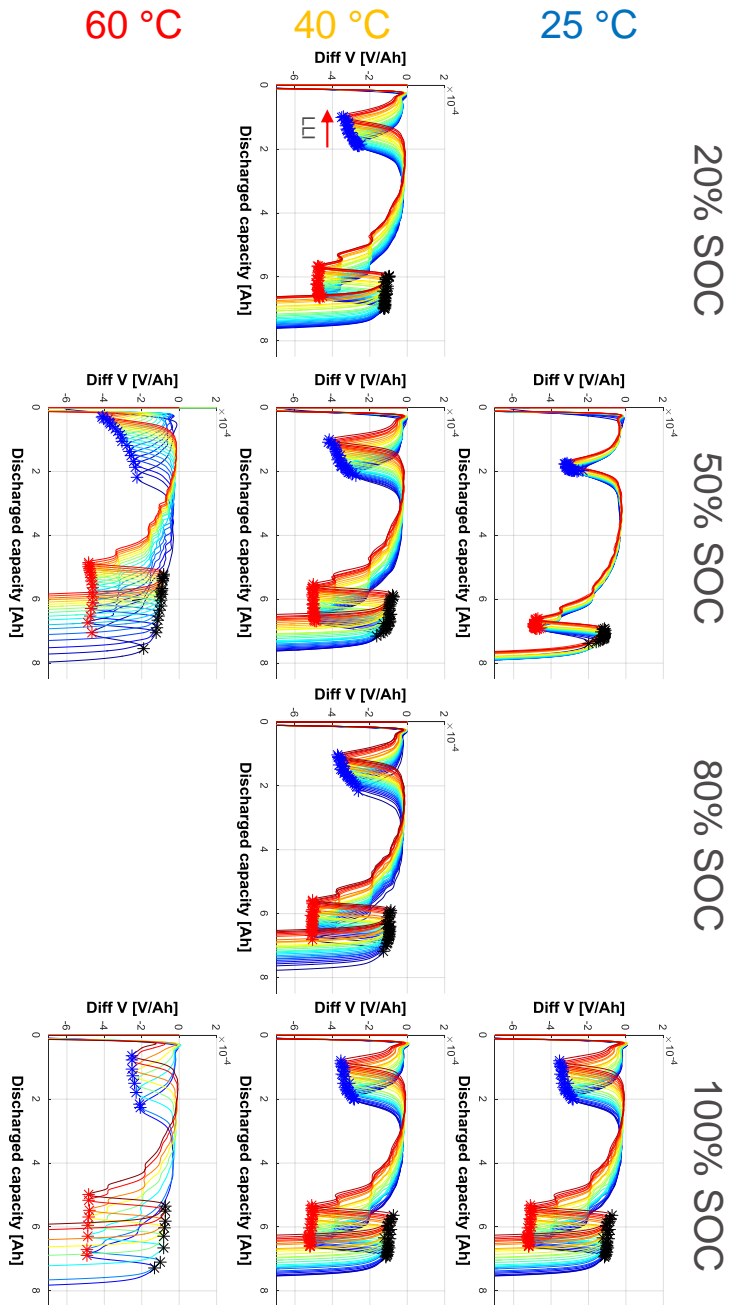


**Figure 2** Series of DVA curves for calendaric aging. Capacity fade increases from blue to red-colored curves. The characteristic points of MinHi (blue), MinLo (red) and MaxLo (black) are highlighted.

The DVA results of each calendaric aging test condition are presented in Figure 2, and DVA results for the cyclic aging tests are shown in Figure 3. Each check-up is represented by one DVA curve, respectively. Capacity fade increases from blue to red-colored curves. All DVAs start at 0 Ah so that the trend of MinHi marked in blue stars is recognizable. Additionally the

maximum at low SOC (MaxLo) is marked in black, and the minimum at low SOC (MinLo) is marked in red. In both figures only the most homogeneous cells are chosen to avoid influence of e.g. inhomogeneous coating. The inhomogeneous cells are discussed in the last section 4.2.3.

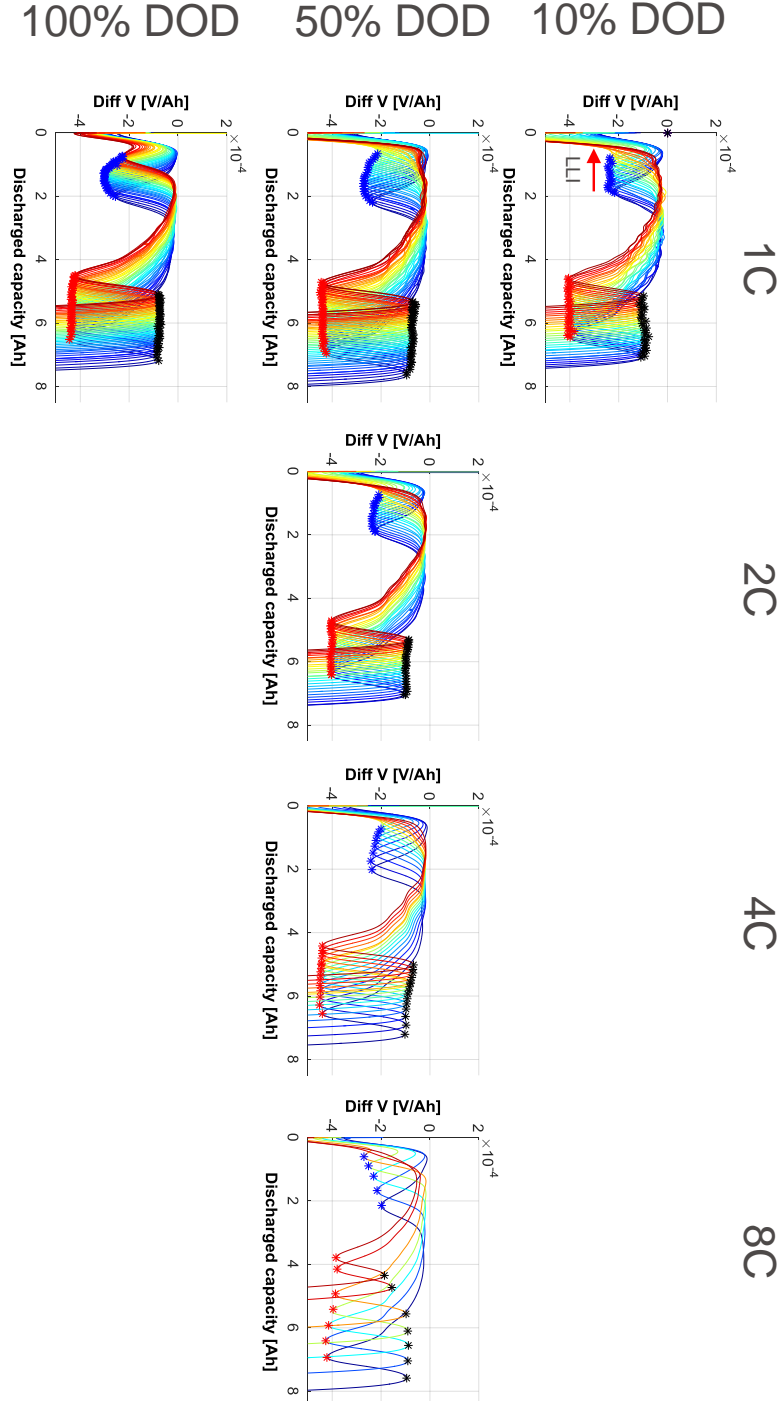


**Figure 3 Series of DVA curves for cyclic aging. Capacity fade increases from blue to red-colored curves. The characteristic points of MinHi (blue), MinLo (red) and MaxLo (black) are highlighted.**

## 4. Discussion

### 4.1 Calendaric aging

#### 4.1.1 Lithium distribution and loss of lithium

Within the first few check-ups of the calendaric aging tests the shape of the DVA becomes sharper and two shoulders around 6-7 Ah appear (Figure 4b). This effect cannot be correlated to certain temperatures or SOCs of the tests. Some cells show a sharp curve already at the first check-up while other cells' curves become sharper over the course of up to eight check-ups.

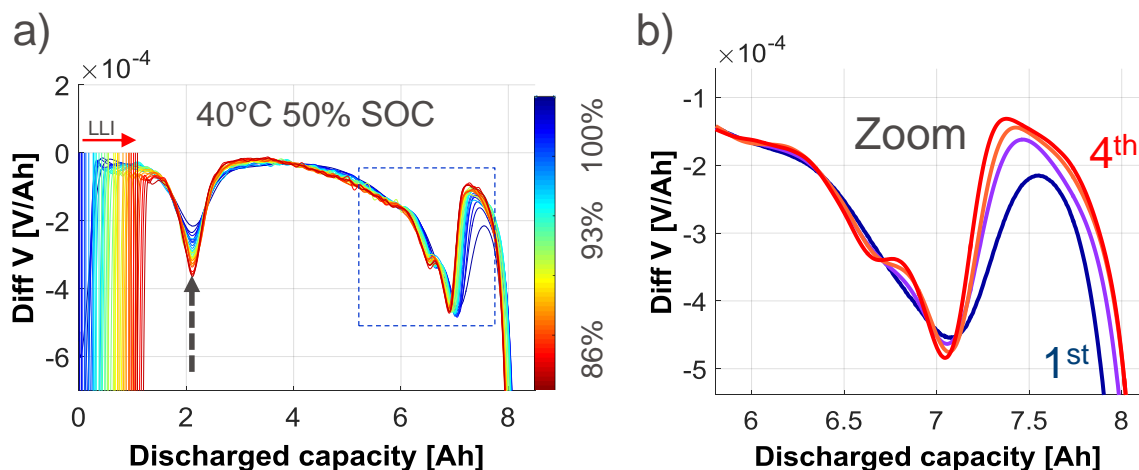


Figure 4 a) The series of DVA for a 40 °C and 50% SOC test is shown exemplarily. Capacity fade increases from blue to red-colored curves as displayed in the color bar. The curves are shifted until all MinHi are arranged with the same Ah-position (marked with an arrow). b) A zoomed view marked in a blue rectangle in a) on the first 4 check-ups.

A reasonable cause of this phenomenon could be that the HLD of the cell itself is comparably low before the test is started. Cells stored at open circuits for an undefined period of time before test start will provide an HLD according to the local potentials of the anode's and cathode's active materials [2]. During the charging and discharging process at check-up, the HLD is affected by additional cell constraints. These are e.g. the local area loading of the

active materials, different local pressure due to inhomogeneous coating, current collector thickness divergences or porosity variations. Thus, under the new constraints the lithium distribution is adapted or homogenized while the cell is cycled slowly during check-ups. To our knowledge, a distinct publication supporting the influence of these constraints is missing in literature.

HLD within a full cycle during the check-up occurs when the slope in the voltage curves of one electrode is remarkably high compared to the counter electrode. This is the case at end of discharge on the anode with a high potential slope while the slope of the cell potential on the cathode is close to zero. Under these conditions particles with a different SOC exhibit a high potential difference and try to compensate at a relatively high velocity. This description of the effect is comparable to the explanation of the passive electrode effect [2]. A similar effect occurs reaching the fully charged state, where hardly any potential difference can be found with respect to the anode while the cathode's potential reveals a high slope.

A typical example of a calendaric aging test conducted at 25 °C and 40 °C is given in Figure 4a (40 °C and 50% SOC). After the previously described increase of HLD from the 1<sup>st</sup> to the 8<sup>th</sup> check-up, the curve shape remains almost constant and the anode can be successively charged to a lower degree of lithiation, so that MinHi will disappear when reaching 75-80% remaining capacity. As  $\Delta$ Minima remains constant the calendaric aging tests at 25 and 40 °C are featured by the loss of active lithium as the major aging mechanism (Figure 2).

Figure 2 shows the DVA results of the calendaric aging for each test condition. For all cells in all calendaric test conditions, MinHi becomes successively sharper, which can be seen in a lowering trend of MinHi marked with blue stars in Figure 2. The sharpening of MinHi is an indicator for an increasing HLD within the entire graphite active material with respect to lithiation or coated specific capacity. This effect is reported in other publications [21,20], while a discussion about this effect is missing. With respect to testing time all cells behave rather homogeneously considering relative representation (results not reported in this work), with the exception of the cells aged at 60 °C and 50% SOC where the sharpening process is

faster. For these cells the internal resistances rise up to 150%. If the aging occurs homogeneously, only an offset of the voltage trend and with this no influence on the characteristic curve shape is expected. In general, this is the case for all cells of the calendaric aging tests. At 60 °C, Fe dissolution from the cathode has to be considered, too (section 4.1.2). The sharpening of MinHi is not influenced by loss of active lithium as the same sharpening is achieved at different states of capacity loss.

In a nutshell, a homogenization effect on the anode with respect to lithium-ion distribution can be observed while the anode active material is not suffering from degradation. Within the first check-ups for some cells the lithium distribution is sufficiently inhomogeneous to establish a high degree of homogeneity within one cycle, whereby this homogenization is observable by the sharpening of MinLo and the MinLo shoulders (Figure 4b). The HLD will be driven by high voltage slopes at end of charge on the cathode and at end of discharge on the anode. These high voltage slopes lead to high lateral currents caused by a high potential difference of inhomogeneously charged particles [6]. When the anode exhibits a high degree of HLD, MinLo and MinLo shoulders remain nearly constant and only the sharpening of MinHi at low anode potential is measurable.

#### **4.1.2 Fe deposition and active material**

Only for the 60 °C cells  $\Delta$ Minima decreases as shown in Figure 5a for a representative cell aged at 50% SOC. In fact, two distinct phases are eye-catching in Figure 5b-c. The first phase is observable up to 50-100 days and the second phase after 50-100 days. For 50% SOC (not graphically shown) and 100% SOC the slope of capacity loss is in the first phase higher than in the second phase. A comparable trend can be observed for  $\Delta$ Minima. For both phases the values of the slopes of the capacity loss and the  $\Delta$ Minima are summarized in Table 3. The slope of  $\Delta$ Minima can be correlated to the trend of the internal resistance in Figure 5c where a saturated value in the range of 50-100 days for all 60 °C tests is reached [2].

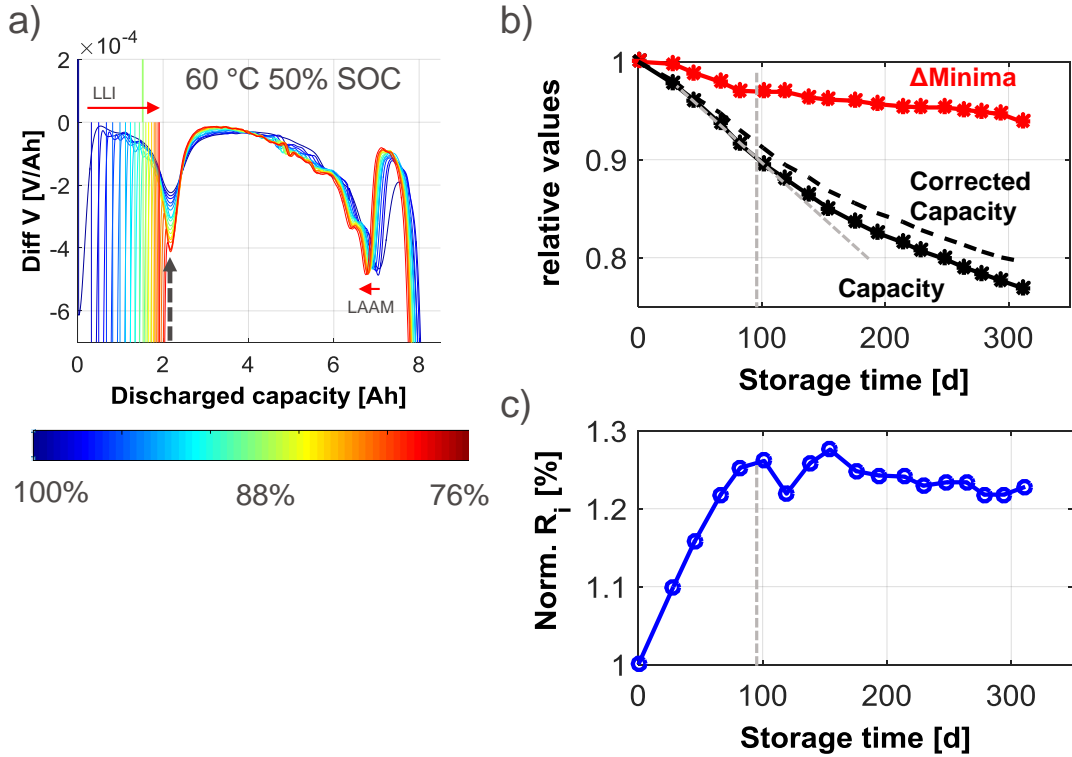


**Figure 5** Representation of a cell aged at 60 °C and 50% SOC. a) DVA series showing sharpening of MinHi, LLI and LAAM. Capacity fade increases from blue to red-colored curves as displayed in the color bar. b) Representation of  $\Delta\text{Minima}$  and capacity loss; c) increase of internal resistance vs. time. Additionally the correction of the capacity loss according to the theory of pores clogging with Fe deposition is included in a dashed line to b).

ICP measurements that have already been presented for these cells [2] exhibit that dissolved Fe from the cathode is found on the anode at 100% SOC and less pronounced under 50% SOC. This is in good correlation to literature where the Fe dissolution is reported especially at high temperatures in the order of 60 °C [22]. The results are summarized in Table 3 where Fe measured on the anode ( $\text{Fe}_A$ ) is normalized to Fe measured on the cathode ( $\text{Fe}_K$ ). In contrast to a catalytic approach it is more likely that the impact per deposited Fe on the capacity loss decreases if Fe has already been deposited. This can be demonstrated by comparing the relative increase of Fe content with the relative increase of  $\Delta\text{Minima}$  at 50% and 100% SOC:  $\Delta\text{Minima}$  decreases by only 75% meanwhile the Fe content increases by

400-700%. Moreover, the reduced rate of capacity loss from the first to the second phase supports the conclusion that Fe does not act in a catalytic way.

The Fe found on the anode does not lead to a measurable loss of capacity of the cathode measured with half-cells. All these findings correlate well to the findings of Li et al. [18]. The authors report LAAM as well and state the Fe deposition on the anode as the reason for the LAAM [18]. It is assumed that the Fe clogs the pores of the graphite in a fully delithiated state so that the clogged active material is deactivated for charge and discharge processes. Nevertheless this theory is not well-proved by experiments. To our knowledge, only Raman measurements of the electrode's surface indicate that the disordered state increases when the  $\Delta$ Minima decreases [18]. However, Raman has only a low penetration depth so that only the surface of the anode is measurable.

**Table 3 Correlation of capacity loss rate  $C_{loss}$  and LAAM by evaluating the reduction of  $\Delta$ Minima for test cells aged at 60 °C and the Fe deposition on Anode  $Fe_A / Fe_K$ .**

	Phase 1		Phase 2		$Fe_A / Fe_K$
	$C_{loss}$	$\Delta$ Minima	$C_{loss}$	$\Delta$ Minima	
50% SOC	8-9	4-5	5-7	1-2	0.1%
100% SOC	18-20	7-8	12	3	0.4-0.7%

In one of the works presented recently by some of the authors for the same cells [13], it was demonstrated that the deposition will not take place in the fully discharged state, but in the corresponding SOC of the calendaric aging test (partially lithiated state). In particular, charging currents (floating currents) to keep 3.6 V are evaluated for the 100% SOC tests. It was found that there is a high correlation between floating currents and the rate of capacity loss. Thus, especially for the 60 °C test condition, Fe dissolution and deposition will take place in the corresponding SOC of the test and not during the intermediated check-ups. It can therefore be safely assumed that, the LAAM will be accompanied by loss of active lithium in the corresponding degree of lithiation. The aging at 100% SOC will therefore be

higher than at 50% SOC; on the one hand because the degree of lithiation of the anode is higher and on the other hand because more Fe is dissolved for higher cell voltages.

In the case that the pores are clogged following the same trend as  $\Delta Minima$  is reduced, the impact on the loss of active lithium and thus the loss of capacity can be calculated according to the following equation for the 50% and 100% SOC:

$$\frac{d}{dt} C_{loss}^{LAAM} = \frac{d}{dt} \Delta Minima(t) \cdot C_{actual}^{avg}(t) \cdot TestSOC \quad (3)$$

Thus, the residual loss of capacity  $C_{loss}^{Residual}$  is calculated as follows and is added to Figure 5b in a dashed line:

$$C_{loss}^{Residual} = C_{loss} - C_{loss}^{LAAM} \quad (4)$$

As can be observed in Figure 5b, the corrected capacity loss still exhibits the previously described two phases instead of a pure linear aging. This means that the aging at 60 °C is not simply the superposition of constant LLI and active lithium clogged in pores, as according to calendaric aging pure LLI follows a linear behavior. The deposition of Fe in the first phase will potentially lead, additionally to clogging of the pores, to a destabilization of the SEI and with this to an increased LLI. In the second phase the Fe might be deposited on top of the previously deposited Fe, leading to less degradation by clogging pores and damaging SEI. Most likely this will be the case on the anode facing the separator. Following this explanation, the nearly constant course of the internal resistance could be explained, too.

## 4.2 Cyclic aging

### 4.2.1 Lithium distribution and loss of lithium

The analysis of the homogeneity phenomenon for cyclic aging presents some differences in comparison with the solely increasing HLD obtained for calendaric aging. This is due to the fact that even small inhomogeneities of the coating, winding etc. will add up during cycling. In return, homogenization forces during rest periods are missing. Only for tests at high DOD, steep voltage slopes are reached, leading to comparably high compensation currents as discussed before. Therefore, the active lithium is assumed to be less uniformly distributed compared to the cells aged calendarically.

In analogy to the calendaric aging tests the HLD is measured according to the sharpness of MinHi and the results are presented in Figure 3 for each test condition. Similar to the evaluation carried out for the calendaric aging, the sharpness is characterized by the trend of MinHi marked with blue stars. Comparing the beginning of the different DODs at a current rate of 1C, MinHi gets sharper with increasing DOD as the sorting potential slope of the anode and cathode increases with DOD as well. At 10% DOD, a constant value for MinHi is measured while after the previously described sharpening at 50% and 100% DOD, MinHi flattens. At 100% DOD this can be referred to inhomogeneously distributed LAAM, as will be discussed in the following section. For the 50% DOD tests the flattening of MinHi will be caused by slow lithium plating [6] on the anode facing the separator. The plated lithium is passivated by the electrolyte resulting in the formation of a covering layer, which is impermeable to lithium-ions as shown in [6]. This leads to inhomogeneous lithium distribution due to e.g. pressure constraints shown in [6] and discussed in depth in section 4.2.3.

At 50% DOD MinHi seems to flatten up to 4C. At 8C MinHi gets sharper. The reason for this behavior could be that at 8C at first the inhomogeneous parts degrade, while from 1C to 4C deposition on top of the anode takes place that decreases HLD. As the cells are kept at a temperature of 40 °C at the cell's case, the temperature in the core especially at 8C will be significantly higher. If this temperature would reach values around 60 °C, the trend of MinHi

might be comparable to the calendric aging tests at 60 °C that reveal a fast sharpening, too. Additional well-designed experiments are necessary to understand this phenomenon in depth.

#### 4.2.2 Electrical decontacting of anode active material

First of all, the influence at a constant current rate of 1C is discussed. At lower DOD ranges between 25% and 75% SOC (50% DOD), no significant loss of graphite according to  $\Delta$ Minima is observable (Figure 6b). At a DOD of 100% a continuous LAAM is measured (Figure 6a) in the order of 0.6-0.7% per 1% point loss of capacity or 4.5- 5% per 1000 FCE. The LAAM is associated with volume expansion and contraction of the anode [23]. In [12] the LAAM is depending on DOD and is hardly measurable up to 60% DOD but quite strong at 100% DOD. A cell described in [12] cycled at 1C and 100% DOD over 3,276 FCE reveals a LAAM of  $\approx$ 19%, graphically obtained by us. This corresponds to a LAAM of 5.8% per 1000 FCE, matching the results obtained in this publication very well. According to the findings of e.g. Hahn et al. [11] there is a strong volume expansion at low and high degrees of lithiation ( $\text{Li}_x$  of  $x = 0\text{-}0.25$  and  $x = 0.55\text{-}1$ ). This results in a low volume change in the SOC range of about 30-65% for this cell. Thus, only 100% DOD exceeds this SOC range of low anode volume work significantly. Therefore, the volume work can be associated to LAAM.

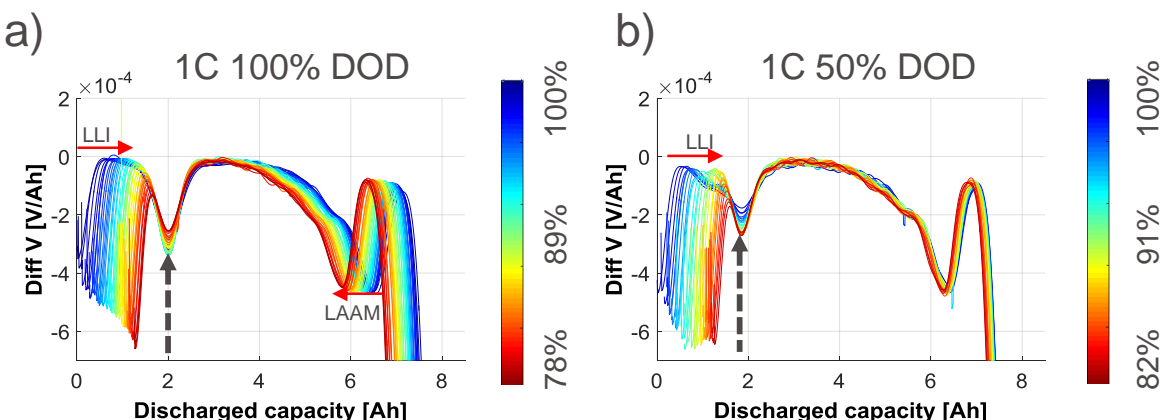


**Figure 6 Series of DVA curves. Capacity fade increases from blue to red-colored curves as displayed in the color bar. In a) the results for a cell aged at 1C and 100% DOD and in b) the results for a cell aged at 1C 50% DOD are plotted.**

If the lost graphite in the cell aged at 1C 100% DOD does not contain any active lithium, no influence on the extractable capacity is expected [21,14]. The reason is that the percentage loss of graphite would need to overcome the oversize factor of  $\frac{c_{anode}}{c_{cathode}} = 1.2$  of the active anode compared to the cathode (measured by half-cell tests) and additionally the loss of capacity of  $LLI_{(Aging+Formation)} = 22\%$  (Figure 6a color bar) which will be mostly LLI during formation and aging. Therefore, the following equation needs to be fulfilled before the LAAM of a fully delithiated graphite would cause a loss of capacity.

$$LAAM > \left[ LLI_{(Aging+Formation)} + \left( \frac{c_{anode}}{c_{cathode}} - 100\% \right) \right] \quad (5)$$

This results in approx.  $LAAM > 22\% + (120\% - 100\%) = 42\%$ , which is by far higher than the LAAM of 20% resulting from the evaluation of the  $\Delta$ Minima for the cell aged at 1C and 100% DOD. According to our previous work, evaluating the capacity loss for the same cells [2], the 100% DOD tests have in average a higher capacity loss of 0.5% per 1000 FCE compared to the 50% DOD tests. Therefore, it is likely that the graphite will be lost in a rather delithiated state of  $\frac{0.5\%}{1000 FCE} \cdot \frac{1000 FCE}{5\%} = 10\%$  in average, assuming that the residual aging remains constant at 50% and 100% DOD. However, at higher voltage the additional contribution of the cathode due to Fe dissolution [18] will reduce the calculated value, so that it should be interpreted as an upper limit.

However, for the cell aged at 100% DOD the half-cell measurements of the graphite anode vs. lithium exhibit a rather low loss of capacity. The normalized capacity decrease starts from 0% in the inner and middle part of the jelly roll<sup>1</sup> and reaches 9% at the outer part of the jelly roll<sup>2</sup>. Furthermore the half-cell measurements are performed on the anode facing inside, which exhibits a higher curvature than the anode facing outside. Keeping previous findings in mind, the LAAM takes place in a rather discharged state of 10% and is located in a low state of pressure regarding graphite expansion due to lithiation. It would therefore be plausible that

---

<sup>1</sup> Position: 70 cm from the core and middle of length about 180 cm

<sup>2</sup> Position: 70 cm to the very end/outside of the 369 cm long anode.

the degradation of anode active material is increased where the mechanical counter pressure due to setup constraints is comparably low. This is the case if the curvature of the winding is higher (facing outside), towards the edges with respect to the electrode's height and at the end of the jelly roll as here the friction counteracting the volume expansion is the lowest. Unfortunately these positions were not measured or are not measurable, so that the discussed theory needs to be justified in future contributions.

Another indicator for local, instead of homogeneous, LAAM is the trend of sharpness of MinHi for the cells aged at 1C and 100% DOD, as already shown in Figure 3. In the first step, MinHi begins to sharpen until the trend changes to a flattening of MinHi. The full cycles themselves lead to an increasing HLD due to the high potential differences at the end of charge and discharge. The local LAAM counteracts this trend and leads to a decreasing HLD, which can be seen by the rising trend of the blue stars in Figure 7b, too.

The presented findings correlate to the theoretical and practical work, found in literature by Sethuraman et al. [24] and Christensen et al. [25] who stated that LLI takes place mostly in low lithiation states  $\text{Li}_x\text{C}$  ( $0 \leq x < 0.16$ ) corresponding to low SOC of 0-20%. They claim that the stress of insertion of lithium-ions in a graphite particle at low lithiation states is the highest so that the decontacting will take place at lower SOCs.

One could assume that the LAAM would not mainly result from the deactivation of particles by losing electrical contact but from the cracking of graphite particles to significantly smaller sizes. In this case, the residual electrically connected graphite particles would be smaller and therefore the size of the particles would be closer to hard carbons. Hard carbons are featured by a smooth voltage curve that does not show any plateaus [26], so that  $\Delta\text{Minima}$  is not measurable due to the missing characteristic minima. However, in that case the characteristic shape of the curve would flatten over the entire DVA, which means that also MinLo and MaxLo would flatten. This is obviously not the case. Finally, this explanation is not supported by the results.

#### 4.2.3 Non-compensating inhomogeneities and electrode deactivation

In a previous publication related to the same cells [10], the formation of a covering layer was observed. The formation of a covering layer could not directly be correlated to a certain aging condition. However, for each of the following three cells aged at 2C and 50% DOD, 1C and 10% DOD and 1C and 100% DOD a covering layer was found to be very pronounced [6]. The DVA representations for these three exemplary cells are given in Figure 7. The graphs on the left, indexed with 1, are all starting at 0 Ah so that the aging due to LLI leads to shifts of the characteristic points to the left. The sharpening of MinHi can be observed when the blue stars reach lower values.  $\Delta\text{MinMax}$  is visible in absolute representation by the distance between the red and the black stars. The graphs on the right, indexed with 2, include capacity loss (black),  $\Delta\text{MinMax}$  (red) and  $\Delta\text{Minima}$  representing LAAM (blue). The additional findings for these cells, considering post-mortem-analysis, capacity fade and increase of internal resistance, are published in [6] and are recapped in the following.

The disassembled 2C and 50% DOD cell reveals a compact covering layer on both sides of the double-sided anode at end of test. This layer is situated in the central part across an area of about 30%. The sudden increase of internal resistance and the decrease of capacity correlate to the covered area. Therefore, the covering layer is supposed to be an electrical insulator and not permeable to lithium-ions. As a consequence, the covered anode and the opposed cathode are successively deactivated and are no longer available for direct charge or discharge. This theory is supported by the ICP measurements, where more active lithium was found on the cathode than it was expected by the remaining capacity results [6].

In the DVA representation in Figure 7a<sub>2</sub>, after around 1000 FCE a sudden reduction of  $\Delta\text{Minima}$  can be observed as well. It starts shortly after the slope of the capacity loss increases. The sudden drops of  $\Delta\text{Minima}$  and capacity loss can be associated to the deactivation of parts of the electrodes, while for LiFePO<sub>4</sub> the loss of cathode active material is not directly measureable with DVA due to missing characteristics. The distance between the minimum and maximum at low SOC  $\Delta\text{MinMax}$  can be observed in Figure 7a<sub>1</sub> according

to the distance of the black and red stars and by the red curve in Figure 7a<sub>1</sub>. The trend of  $\Delta\text{MinMax}$  is reducing at first until it starts rising again. The reduction of  $\Delta\text{MinMax}$  is associated with an increasing inhomogeneity that cannot be equalized at end of charge or during discharge by potential differences. Therefore, the initial open-pore deposition of the covering layer leads to faster discharge of uncovered parts and to slower discharge of covered parts, resulting in flattening of the curve, which increases with longer discharge time. When the remaining pores are filled and the larger areas of the covering layer start to become compact, the covered anode and the opposed cathode are successively deactivated. Thus, the area of the covered part is growing and cannot be measured during discharge anymore, so that the lithium distribution during the DVA measurement is homogenizing again. This behavior correlates perfectly to the described theory, illustrated in figure 8 in [10] for these cells, and to the analysis of increase and decrease of capacity difference (CDA) measured at 0.25C and 1C. Moreover, the shape of MinHi (Figure 7a<sub>1</sub> blue) shows in the beginning a sharpening due to increasing HLD by potential differences on the anode during cycling. As the covering layer evolution starts, the minimum flattens until it sharpens again when the covering layer becomes impermeable to lithium-ions.

Comparable findings are observed for the cell aged at 1C and 100%. The cell is disassembled in a fully charged state [6]. The covering layer deposited on the anode is less pronounced and is present on one side of the electrode only. On the direct back side of the covering layer in the cell's center, golden-colored particles are observed in an area of about 17% of the total geometrical surface of the anode. In [6] it was announced that the increasing pressure of the covering layer leads to a charge agglomeration at its back side, resulting in overcharging and development of a covering layer. The remaining 39% extractable capacity at the end of test seems not to provide enough active lithium to overcharge the back side and form a second covering layer.

In the DVA in Figure 7b<sub>1</sub> (distance between black and red stars) and in Figure 7b<sub>2</sub> (red)  $\Delta\text{MinMax}$  decreases only as the high-charged part of the back side is not equalized with the

low-charged parts of the anode during end of charge and end of discharge. Instead, due to the pressure of the other side of the anode, the inhomogeneity of lithium distribution increases at end of discharge during cycling, as described in the previous section. Additionally, the actual discharge rate at end of test for the DVA locally reaches about 1.5C instead of 0.25C due to the better accessible electrode, which might lead to some extent to an additional flattening of the characteristic peaks MinLo and MaxLo. From the beginning,  $\Delta\text{Minima}$  decreases continuously by decontacting of active material, as explained in the previous paragraph in Figure 6. The additional loss of  $\Delta\text{Minima}$  due to covering layer evolution is not measurable as the covering layer evolution starts at about 70% remaining capacity, while MinHi disappeared at about 80%.

The 1C and 10% DOD cell reveals a covering layer, too. The reasons for the evolution of the covering layer at these safe SOC, with respect to lithium plating conditions, are not yet fully understood. As there is hardly any potential slope in the cycling range neither on the cathode nor on the anode (see Figure 1b-c), an inhomogeneous lithium distribution is not balanced out during cycling and might locally lead to lithium plating by overcharging during check-up. However, the DVA for this cell shows a reducing value of  $\Delta\text{MinMax}$  from 90% remaining capacity on (Figure 7c<sub>2</sub> (red)). With a short delay the slope of capacity loss is increasing again.  $\Delta\text{Minima}$  exhibits some fluctuations but unfortunately, shortly after the slope of capacity declines stronger,  $\Delta\text{Minima}$  is no longer evaluable. Moreover, for 1C and 10% DOD the homogeneity decreases as shown in Figure 7c<sub>1</sub> (blue). From 1,500 FCE on, the decrease of capacity is additionally associated with covering layer formation.

Summarizing, the characteristic trend of  $\Delta\text{MinMax}$  gives information about strongly inhomogeneous lithium distribution, resulting from e.g. deactivated electrodes due to dense covering layer, pressure inhomogeneities or strongly inhomogeneous coating or aging. If a reduction of  $\Delta\text{MinMax}$  is accompanied by an increased capacity loss, lithiated electrodes are successively deactivated by a covering layer.

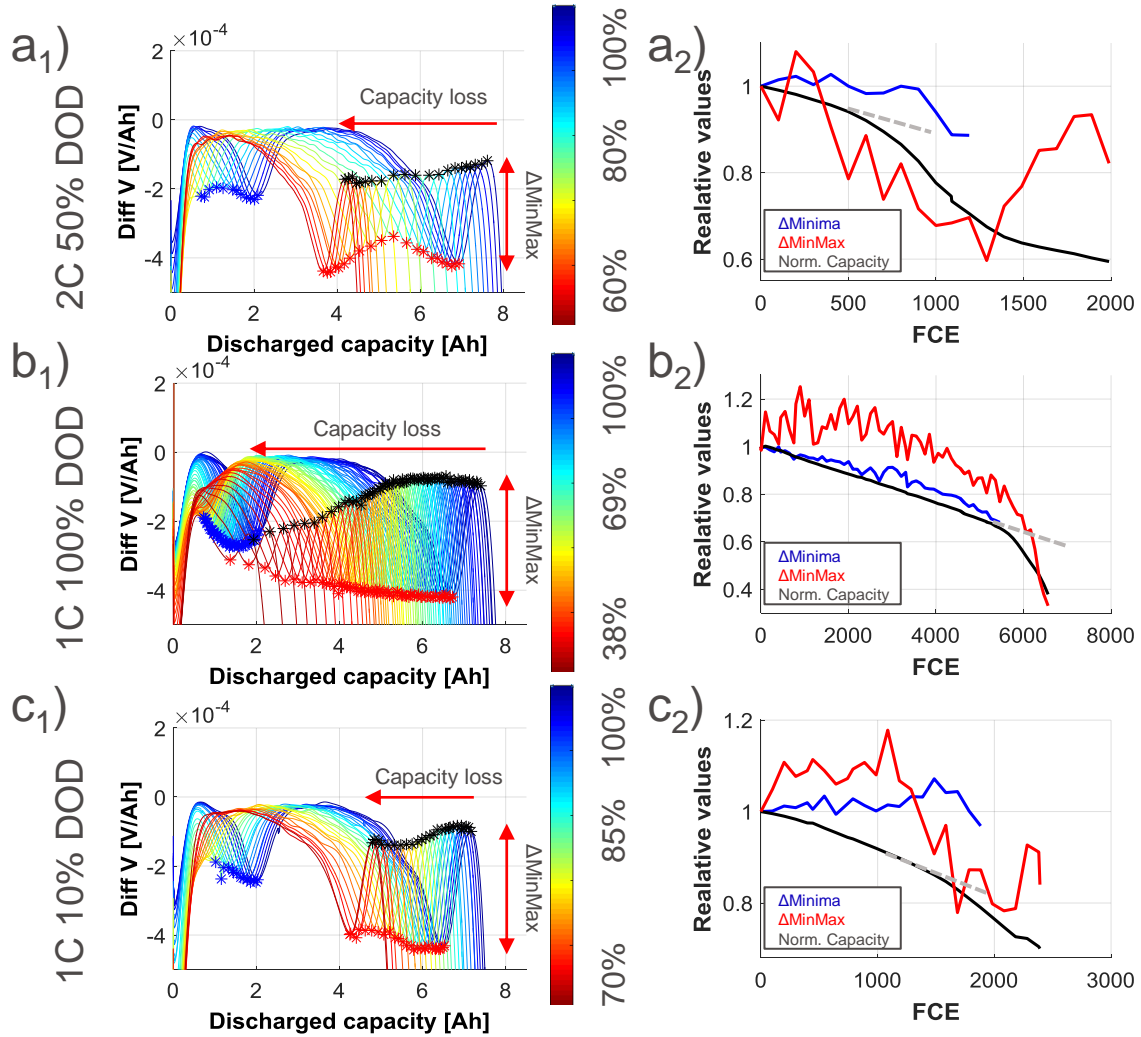


**Figure 7** Characteristic aging curves for a) 2C and 50% DOD, b) 1C and 100% DOD and c) 1C and 10% DOD. Left: Series of DVA curves starting at 0 Ah. Capacity fade increases from blue to red-colored curves as displayed in the color bar. Right: Capacity loss (black),  $\Delta\text{MinMax}$  (red) and  $\Delta\text{Minima}$  (blue) vs. FCE. The grey dashed line shows at which capacity the influence of the covering layer is measurable.

## Conclusions

Using the differential voltage analysis, a trend of increasing homogeneity of lithium distribution can be measured with three characteristic points. The highest sensitivity is revealed by the sharpness of MinHi, followed by the appearance of the shoulders of the peak at MinLo. If the anode exhibits two or more disjunctive lithium concentrations, the distance  $\Delta\text{MinMax}$  between minimum and maximum at low SOC decreases.

For all cells of the different calendaric aging tests the homogeneity of lithium distribution increases with aging. Up to 40 °C the cells age solely by loss of active lithium; at 60 °C additional loss of capacity measured by reducing  $\Delta\text{Minima}$  needs to be considered. The LAAM is associated with the deposition of dissolved Fe from the cathode on the anode. The influence of the LAAM on capacity fade could be quantified assuming that the pores are clogged in the degree of lithiation during storage. However, after subtracting the estimated influence of LAAM, two slopes of capacity fade are still present, showing that there is another contribution to aging. As the influence of the deposited Fe on the LAAM decreases, the Fe is most likely deposited on previously deposited Fe and will therefore not clog additional pores of the anode. The higher slope of capacity fade in the beginning might be attributed to high reactivity of the first deposited Fe with active lithium.

With respect to cycling, operating the cells at 100% DOD leads to continuous LAAM. The active material is lost in a low state of charge of less than 10%, as calculated from the higher average capacity fade, compared to 50% DOD test without LAAM. The LAAM is assumed to be inhomogeneously distributed, while the higher losses should be located where the mechanical pressure in the cylindrical cell is the lowest: edgewise at the anode overhang, outer windings and anode facing outside. This is supported by continuously reducing homogeneity measured according to flattening of MinHi.

The evolution of a covering layer is detectable when a sudden strong reduction of capacity occurs, while  $\Delta\text{Minima}$  and  $\Delta\text{MinMax}$  decreases and MinHi flattens. The increasing

inhomogeneous lithium distribution could be linked to a locally increasing path length, due to masking or to locally increased pressure caused by covering layer on top of the anode. The capacity loss and the LAAM result from deactivation of anode and cathode, whereby only LAAM is measurable as loss of cathode active material is not directly detectable with DVA, due to missing characteristics. Furthermore loss of cathode active material has only an influence on capacity loss, in the way it is lithiated.

## Acknowledgement

The results were generated during the project MEET-HiEnD. We like to thank the ‘Bundesministerium für Bildung und Forschung’ (BMBF) for funding (03X4634B).

## Literature

- [1] J. Cannarella, C.B. Arnold, Stress evolution and capacity fade in constrained lithium-ion pouch cells, *J. Power Sources.* 245 (2014) 745–751.  
doi:10.1016/j.jpowsour.2013.06.165.
- [2] M. Lewerenz, J. Münnix, J. Schmalstieg, S. Käbitz, M. Knips, D.U. Sauer, Systematic aging of commercial LiFePO<sub>4</sub>/Graphite cylindrical cells including a theory explaining rise of capacity during aging, *J. Power Sources.* 345 (2017) 254–263.  
doi:10.1016/j.jpowsour.2017.01.133.
- [3] B. Gyenes, D.A. Stevens, V.L. Chevrier, J.R. Dahn, Understanding Anomalous Behavior in Coulombic Efficiency Measurements on Li-Ion Batteries, *J. Electrochem. Soc.* 162 (2015) A278–A283. doi:10.1149/2.0191503jes.
- [4] M. Klett, R. Eriksson, J. Groot, P. Svens, K. Ciosek Höglström, R.W. Lindström, H. Berg, T. Gustafson, G. Lindbergh, K. Edström, Non-uniform aging of cycled commercial LiFePO<sub>4</sub>//graphite cylindrical cells revealed by post-mortem analysis, *J. Power Sources.* 257 (2014) 126–137. doi:10.1016/j.jpowsour.2014.01.105.

- [5] P.J. Osswald, S. V Erhard, A. Rheinfeld, B. Rieger, H.E. Hoster, A. Jossen, Temperature dependency of state of charge inhomogeneities and their equalization in cylindrical lithium-ion cells, *J. Power Sources.* 329 (2016) 546–552.  
doi:10.1016/j.jpowsour.2016.08.120.
- [6] M. Lewerenz, A. Warnecke, D.U. Sauer, Post-Mortem Analysis on LFP|Graphite cells describing the evolution & composition of covering layer on anode and their impact on cell performance, *J.Power Sources.* 369 (2017) 122–132.  
doi:10.1016/j.jpowsour.2017.10.003.
- [7] M. Klett, P. Svens, C. Tengstedt, A. Seyeux, S. Jolanta, G. Lindbergh, R. Wreland, Uneven Film Formation across Depth of Porous Graphite Electrodes in Cycled Commercial Li-Ion Batteries, *J. Phys. Chem. C.* 119 (2015) 90–10.  
doi:10.1021/jp509665e.
- [8] B. Stiaszny, J.C. Ziegler, E.E. Krauß, J.P. Schmidt, E. Ivers-tiffée, Electrochemical characterization and post-mortem analysis of aged  $\text{LiMn}_2\text{O}_4\text{eLi}(\text{Ni}_0.5\text{Mn}_0.3\text{Co}_0.2)\text{O}_2$ /graphite lithium ion batteries. Part I: Cycle aging, *J. Power Sources.* 251 (2014) 439–450. doi:10.1016/j.jpowsour.2013.11.080.
- [9] J. Cannarella, C.B. Arnold, The Effects of Defects on Localized Plating in Lithium-Ion Batteries, *J. Electrochem. Soc.* 162 (2015) A1365–A1373. doi:10.1149/2.1051507jes.
- [10] M. Lewerenz, A. Warnecke, D.U. Sauer, Introduction of capacity difference analysis (CDA) for analyzing lateral lithium-ion flow to determine the state of covering layer evolution, *J. Power Sources.* 354. (2017) 157–166.  
doi:10.1016/j.jpowsour.2017.04.043.
- [11] M. Hahn, H. Buqa, P.W. Ruch, D. Goers, M.E. Spahr, J. Ufheil, P. Novák, R. Kötz, A Dilatometric Study of Lithium Intercalation into Powder-Type Graphite Electrodes, *Electrochem. Solid-State Lett.* 11 (2008) A151–A154. doi:10.1149/1.2940573.

- [12] E. Sarasketa-Zabala, I. Gandiaga, E. Martinez-Laserna, L.M. Rodriguez-Martinez, I. Villarreal, Cycle ageing analysis of a LiFePO<sub>4</sub>/graphite cell with dynamic model validations: Towards realistic lifetime predictions, *J. Power Sources.* 275 (2015) 573–587. doi:10.1016/j.jpowsour.2014.10.153.
- [13] M. Lewerenz, J. Münnix, J. Schmalstieg, S. Käbitz, M. Knips, A. Warnecke, D.U. Sauer, New method evaluating currents keeping the voltage constant for fast and high resolved measurement of Arrhenius relation and capacity fade, *J. Power Sources.* 353 (2017) 144–151. doi:10.1016/j.jpowsour.2017.03.136.
- [14] M. Safari, C. Delacourt, Aging of a Commercial Graphite/LiFePO<sub>4</sub> Cell, *J. Electrochem. Soc.* 158 (2011) A1123–A1135. doi:10.1149/1.3614529.
- [15] I. Bloom, J. Christophersen, K. Gering, Differential voltage analyses of high-power lithium-ion cells 2. Applications, *J. Power Sources.* 139 (2005) 304–313. doi:10.1016/j.jpowsour.2004.07.022.
- [16] T.G. Zavalis, M. Klett, M.H. Kjell, M. Behm, R.W. Lindström, G. Lindbergh, Aging in lithium-ion batteries : Model and experimental investigation of harvested LiFePO<sub>4</sub> and mesocarbon microbead graphite electrodes, *Electrochim. Acta.* 110 (2013) 335–348. doi:10.1016/j.electacta.2013.05.081.
- [17] P. Keil, S.F. Schuster, J. Wilhelm, J. Travi, A. Hauser, R.C. Karl, A. Jossen, Calendar Aging of Lithium-Ion Batteries, *J. Electrochem. Soc.* 163 (2016) A1872–A1880. doi:10.1149/2.0411609jes.
- [18] D. Li, D.L. Danilov, L. Gao, Y. Yang, P.H.L. Notten, Degradation Mechanisms of the Graphite Electrode in C 6 /LiFePO 4 Batteries Unraveled by a Non-Destructive Approach, *J. Electrochem. Soc.* 163 (2016) A3016–A3021. doi:10.1149/2.0821614jes.
- [19] T.G. Zavalis, M. Klett, M.H. Kjell, M. Behm, R.W. Lindström, G. Lindbergh, Aging in lithium-ion batteries : Model and experimental investigation of harvested LiFePO 4 and

mesocarbon microbead graphite electrodes, *Electrochim. Acta.* 110 (2013) 335–348.

doi:<http://dx.doi.org/10.1016/j.electacta.2013.05.081>.

- [20] I. Bloom, A.N. Jansen, D.P. Abraham, J. Knuth, S.A. Jones, V.S. Battaglia, G.L. Henriksen, Differential voltage analyses of high-power, lithium-ion cells 1. Technique and application, *J. Power Sources.* 139 (2005) 295–303.  
doi:[10.1016/j.jpowsour.2004.07.021](https://doi.org/10.1016/j.jpowsour.2004.07.021).
- [21] I.V. E. Sarasketa-Zabala, I. Gandiaga, L.M. Rodriguez-Martinez, Calendar ageing analysis of a LiFePO<sub>4</sub> / graphite cell with dynamic model validations : Towards realistic lifetime predictions, *272* (2014) 45–57. doi:[10.1016/j.jpowsour.2014.08.051](https://doi.org/10.1016/j.jpowsour.2014.08.051).
- [22] M. Koltypin, D. Aurbach, L. Nazar, B. Ellis, More on the performance of LiFePO<sub>4</sub> electrodes-The effect of synthesis route, solution composition, aging, and temperature, *J. Power Sources.* 174 (2007) 1241–1250. doi:[10.1016/j.jpowsour.2007.06.045](https://doi.org/10.1016/j.jpowsour.2007.06.045).
- [23] J. Vetter, P. Nov, M.R. Wagner, C. Veit, Ageing mechanisms in lithium-ion batteries &, *147* (2005) 269–281. doi:[10.1016/j.jpowsour.2005.01.006](https://doi.org/10.1016/j.jpowsour.2005.01.006).
- [24] V.A. Sethuraman, L.J. Hardwick, V. Srinivasan, R. Kostecki, Surface structural disordering in graphite upon lithium intercalation/deintercalation, *J. Power Sources.* 195 (2010) 3655–3660. doi:[10.1016/j.jpowsour.2009.12.034](https://doi.org/10.1016/j.jpowsour.2009.12.034).
- [25] J. Christensen, J. Newman, Stress generation and fracture in lithium insertion materials, *J. Solid State Electrochemistry.* 10 (2006) 293–319. doi:[10.1007/s10008-006-0095-1](https://doi.org/10.1007/s10008-006-0095-1).
- [26] M. Wilamowska, M. Graczyk-Zajac, R. Riedel, Composite materials based on polymer-derived SiCN ceramic and disordered hard carbons as anodes for lithium-ion batteries, *J. Power Sources.* 244 (2013) 80–86. doi:[10.1016/j.jpowsour.2013.03.137](https://doi.org/10.1016/j.jpowsour.2013.03.137).